

# Convergence of body-orders in linear atomic cluster expansions

Apolinario Miguel Tan,\* Franco Pellegrini, and Stefano de Gironcoli  
*Scuola Internazionale Superiore di Studi Avanzati, Trieste, Italy*  
(Dated: February 25, 2025)

## Abstract

We study the convergence of a linear atomic cluster expansion (ACE) potential [1] with respect to its basis functions, in terms of the effective two-body interactions of elemental Carbon systems. We build ACE potentials with descriptor sets truncated at body-orders  $K = 2, 3, 4$  trained on pure dimers, or on large datasets of different diversities but without any dimers. Potentials trained on a more diverse dataset fare better in validation and result in a nontrivial dimer curve, but still very far from the theoretical two-body interaction calculated by DFT. Moreover, dimer curves between descriptor sets clipped at different  $K$  do not seem to converge to a universal function for a given dataset. We conclude that machine learning potentials employing atomic cluster expansions optimize losses at low  $K$  but fail to generalize and converge properties described by two-body interactions.

## I. INTRODUCTION

Decompositions of the total energy of atomic systems by  $N$ -body contributions, or cluster expansions,

$$E(\{\mathbf{r}_i\}) = V^{(0)} + \sum_i V^{(1)}(\mathbf{r}_i) + \sum_{\substack{i,j \\ i \neq j}} V^{(2)}(\mathbf{r}_i, \mathbf{r}_j) + \sum_{\substack{i,j,k \\ i \neq j \neq k \neq i}} V^{(3)}(\mathbf{r}_i, \mathbf{r}_j, \mathbf{r}_k) + \dots \quad (1)$$

have been used as the framework to study material properties such as the thermodynamics of substitutional alloys [2, 3] and empirical potentials of condensed matter and molecular systems [4–6]. While the infinite expansion has been shown to be complete, its practical effectiveness is limited to cases where the total energy converges after a few body-orders  $\nu$ , as the number of terms increases combinatorially as higher orders are included.

More recently, the expansion has been used in describing local chemical environments for machine learning potentials. The underlying assumption for these descriptors is that the energy of the system is a sum of its individual atomic contributions  $E_i$  [7],

$$E(\{\mathbf{r}_i\}) = \sum_{i=1}^N E_i(\{\mathbf{r}_i\}) \quad (2)$$

where  $N$  indicates the total number of atoms in the structure. The atomic energies may then be expressed as an expansion in the number of neighbors.

Developments on improving the construction of  $E_i$  have been made in recent decades, with symmetry-respecting descriptors that use only a few terms in the expansion [7–10] or take advantage of tensorial operations to reach an arbitrary body order [1, 11–13]. A detailed review on descriptors of local chemical environments has been done by Musil *et al.* [14]

While the completeness [2, 3, 15] of such expansions allow an apt description of the system, its form in Eq. 1 are considered to converge slowly<sup>1</sup> [4, 5, 17], where computing a term of order  $\nu$  would scale in powers of  $\nu - 1$  of the number of neighbors. In order to avoid this prohibitive scaling, it is possible to express higher body-order terms as the product of simple two-body terms, at the price of including lower order terms, and losing the orthogonality of the expansion. A popular version of this resummation is the Atomic Cluster Expansion proposed by Drautz [1]. In this approach, each  $E_i$  is expanded with a non-orthogonal basis,  $\{A_\nu\}$ , with unrestricted sums,

$$E_i(\{\mathbf{r}_i\}) = \sum_\nu c_\nu^{(1)} A_{i,\nu} + \sum_{\substack{\nu_1 \geq \nu_2 \\ \nu_1 \nu_2}} c_{\nu_1 \nu_2}^{(2)} A_{i,\nu_1} A_{i,\nu_2} + \dots \quad (3)$$

with single sums over neighbors

$$A_{i,\nu} = \sum_j f_\nu(\mathbf{r}_i, \mathbf{r}_j), \quad (4)$$

and  $\nu$  indexing the terms of the expansion.

The expansion has been shown to be complete [15], and implementations of the code have shown promise in machine learning applications [18–21]. One of the state-of-the-art potentials, MACE [13], extends from the formalism of ACE and represents the state of the art in molecular dynamics applications for materials with multiple elements [22].

Whereas potentials adopting ACE descriptors have shown to converge fast in losses, a detailed study on the convergence of the body-orders with respect to properties described by lower orders in the original expansion in Eq. 1 have not been thoroughly investigated. In this work, we investigate the convergence of linear ACE at different body-orders  $K$  in terms of their projection on the lowest terms of the original cluster expansion Eq. 1. In

<sup>1</sup> Counterarguments [16] against the speed of convergence of body-ordered expansions claim that the surrounding environments are typically ignored and are usually crucial in the convergence at low body-orders.

\* atan@sissa.it

particular, we consider the convergence of the potential in energy and forces on different datasets, as a function of the number and type of basis functions utilized, and compare it to the stability of a real body ordered expansion. Our study focuses on the first nontrivial term of the expansion: the two-body term. This can be easily extracted from a given potential by studying the energy profile of two isolated atoms, a dimer, as a function of distance:

$$E_{2b,i}(\mathbf{r}_i, \mathbf{r}_j) = V^{(2)}(\mathbf{r}_i - \mathbf{r}_j). \quad (5)$$

It is thus natural to ask whether this function might converge to the real dimer dissociation curve, or to another arbitrary function for a dataset that does not contain dimers.

Neural network potentials (NNPs) may also employ nonlinearities via functional embeddings [6, 23, 24], or are inherent from their activation layers [7, 9, 10, 14, 25]. While nonlinearities improve their performance by being able to represent higher-order terms when the expansion is truncated, one has to be careful in how they are applied as certain applications may invalidate the body-ordering of the descriptor [12]. We do not aim to build the most accurate potentials, but to have a more grounded understanding of their behavior in the ACE framework. As such, we limit our investigations to training simpler linear models as well as not going to too high of a body-order where returns are diminished. Linear ACE models perform comparably well relative to neural network potentials, and have been successfully employed to describe molecular [18] and condensed phases [19].

## II. METHODS

### A. Datasets

The datasets we use in the investigations consists of elemental Carbon structures. Three datasets were used: the first set consists of 247 dimer structures at logarithmically-spaced distance between 0.5 and 8 Angstrom. Half of the structures were randomly selected for the validation set. The remaining two are sets of 1000 structures coming from a collection of Carbon allotropes generated from [26]. One subset contains a homogeneous collection of diamond-like structures clustered using a Euclidean distance measure [27]. The diamond-like dataset is highlighted in the histogram of distances to a reference diamond structure in Fig. 1. The last subset are structures obtained using farthest point sampling [28] to maximize its diversity. For the diamond-like and diverse datasets, a validation set was constructed from 1000 diverse structures that have not been seen in training. All structures studied energies and forces were calculated using the **Quantum Espresso** package [29] using the rVV10 functional [30] to account for nonlocal interactions.

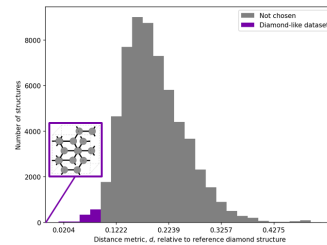


FIG. 1. Histogram of fingerprint distances of the configurations in the Carbon dataset in [26] relative to a reference diamond-like structure (inset). 1000 configurations were chosen within a narrow region in structure space.

### B. Descriptor

We use the ACE descriptor as implemented by the **pacemaker** package [20]. We used scaled Chebyshev polynomials as the radial functions, vanishing smoothly at the cutoff length of  $r_{\text{cut}} = 5 \text{ \AA}$ . We start from  $K = 2$  body functions and progressively add more terms of the same order. We then introduce higher order  $K = 3$  terms while keeping the number of lower order terms fixed, and then repeat the procedure for higher orders. ACE descriptors employ spherical harmonics to describe angular functions, with  $n, l$  values chosen to respect maintain rotational symmetry. Low  $n, l$  values were chosen to avoid overfitting the model from too many basis functions. We note that the original ACE and the current version of **pacemaker** include self-interactions from  $K > 2$  body orders, so redundancies of lower-body order functions appear as functions of higher  $K$ .

### C. Fitting procedure

We use the default loss function  $\mathcal{L}$  of **pacemaker** [20],

$$\mathcal{L} = (1 - \kappa) \Delta_E^2 + \kappa \Delta_F^2 + \Delta_{\text{coeff}} + \Delta_{\text{rad}} \quad (6)$$

where  $\Delta_E^2$  and  $\Delta_F^2$  are the corresponding energy and force root-mean-square errors (RMSE), and  $\kappa$  is the coefficient that balances the energy and force contributions to  $\mathcal{L}$ . The term  $\Delta_{\text{coeff}}$  regularizes the basis function coefficients<sup>2</sup>, while  $\Delta_{\text{rad}}$  regularizes the coefficients of the radial components of the basis function. The dimer dataset was randomly split between training and validation set, while the diamond-like and generic datasets were validated using a set similar to the generic set. To reconstruct the 2-body contribution to the cluster expansion, we build the energy curve of two isolated Carbon atoms as in Eq. 5. The converged potentials from **pacemaker** were evaluated using the Atomic Structure Environment (ASE) code [31].

<sup>2</sup> This term includes the L1 and L2 regularizations.

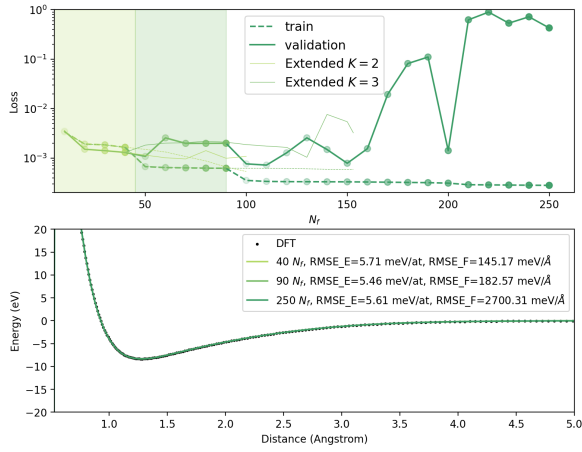


FIG. 2. Top:  $\mathcal{L}$  as a function of number of basis functions,  $N_f$ , for the dimer dataset. Training and validation errors as dashed and solid curves. Curve colors indicate potentials built from basis sets which are exclusively two-body (light green), up to three-body (green), and up to four-body functions (dark green), respectively. Light solid lines indicate  $\mathcal{L}$  if more functions introduced keeping the previous  $K = 2$  or  $K = 3$ . Bottom: dimer curves for each of the potentials trained at certain  $N_f$ , with reference DFT data as points. Heavy lines represent the potential with the largest  $N_f$  before functions of higher  $K$  are introduced.

### III. RESULTS AND DISCUSSION

We start by fitting the dimer dataset with an increasing number of basis functions,  $N_f$ , up to 250 elements and  $K = 4$  body-order. The loss and dimer curves are shown in Fig. 2, where light green, green, and dark green indicate data from potentials trained using  $K$  up to 2, 3, and 4, respectively. The top plot shows the dependence of the loss  $\mathcal{L}$  from Eq. 6 to  $N_f$ . The validation loss (solid curve) converges  $K = 2$  and increases with the addition of higher order functions, jumping two orders of magnitude as more  $K = 4$  functions are added. This is of course to be expected, as the dataset consists solely of 2 body structures. The bottom plot highlights the dimer curves of the potentials trained from the dimer set at the highest  $N_f$  of a particular order  $K$ . We see that all potentials were able to reproduce the dimer curve as expected from the DFT results.

The energy RMSE for the representative potentials were around 5 meV/at, and force RMSE were slightly less than 200 meV/Å for  $K = 2$  and  $K = 3$ . The force RMSEs increased to 2700 meV/Å for the overfitting potential that at  $N_f = 250$ , and are due to the short-range region of the curve having energies up to almost two orders of magnitude higher, making the deviations from DFT results more sensitive to errors. A comparison of the forces at the short range region may be found in the Supporting Information B.1.

The results for the homogeneous diamond-like dataset are shown in Fig. 3. Unlike the potentials trained from

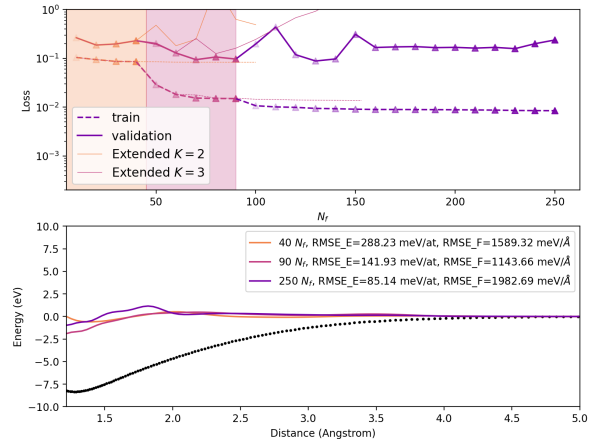


FIG. 3.  $\mathcal{L}$  vs.  $N_f$  (top) and dimer curves (bottom) for the homogeneous, diamond-like dataset. Orange and pink plots correspond to potentials with only  $K = 2$  and up to  $K = 3$  functions, respectively while purple curves include  $K = 4$  functions. The x-values of the dimer curve start at the minimum distance found in the homogeneous dataset.

the dimer dataset, the training loss from the diamond-trained potentials reduce by an order of magnitude upon the introduction of the  $K = 3$  functions. The light orange line indicates that given the same  $N_f$ , the basis set purely constructed from  $K = 2$  functions does not have as pronounced of a decrease in  $\mathcal{L}$ . We see that the validation over the diverse set has losses improving for  $K = 3$ , but overfitting occurs at  $K = 4$ . The dimer curves from these potentials show a considerable amount of variability even after the loss is converged, and they remain far from the expected dimer behavior dictated by DFT. Of course, the lack of diversity in this dataset, leading to very small variations in the radial distribution function, might be part of the reason why a rather flat 2-body curve is obtained. Moreover, the overfitting for the large descriptor size could contribute to the variability of this contribution.

We then look at the dimer curves produced by the diverse dataset for different descriptor complexities, ranging from  $K = 2$  to 5, with various sizes for  $K = 4$  (similar loss analysis with consistent earlier dimer curves are shown in the Supporting Information B.2.). Fig. 4 shows these curves having more pronounced shapes as compared to the ones produced by the diamond-like dataset. While the curves look similar as more functions of the same  $K$  are introduced in the set as seen in the  $K = 4$  potentials, the curves of different  $K$  limits do not seem to converge even when five-body contributions are already added. The variability is much more pronounced, even among potentials with similar maximum  $K$  and more so when adding new terms. We posit that the effective two-body potential does not seem to converge, even for when five-body basis functions are added, leading to an arguably well-converged potential.

Lastly, we train a potential that includes the 50000

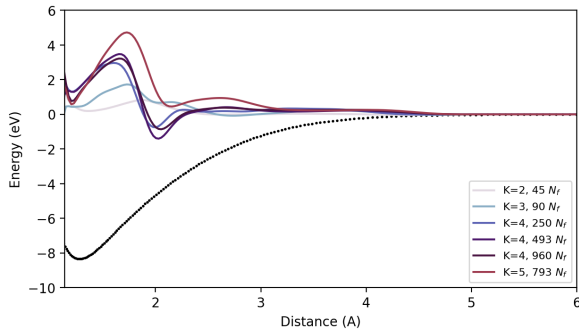


FIG. 4. Dimer curves for the diverse 1000-structure dataset for extended descriptor sizes. While curves produced by models within a certain  $K$  ( $K = 4$ ) may appear to converge, they qualitatively do not seem to approach a consistent shape whenever functions of higher  $K$  are introduced in the descriptor set.

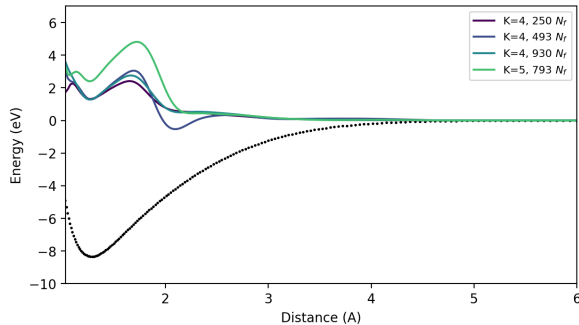


FIG. 5. Dimer curves for expanded 50000-structure dataset for multiple descriptor sizes. Like the potentials trained with a smaller dataset in Fig. 4, potentials trained with increasing descriptor sizes but within a certain  $K$  seem to converge, but introducing the descriptor set with  $K = 5$  basis functions vary the shape considerably.

structures on the whole Carbon dataset in [26] to see if further increasing the complexity of the input data affects our conclusion. The dimer curves shown in Fig. 5 tell the same story as the one of smaller dataset: the curves do not approach the DFT dimer results at all, and they do not seem to converge to a fixed function as higher  $K$  basis elements are introduced.

It is worth reminding that we are testing the generalization capabilities of the diverse set potentials and not their ability to capture in-domain data. The pair-interactions present in the set are those that exist in surrounding materials and not in isolation. A brief test shown in Supporting Information B.3. shows that gradually populating the diverse dataset with dimers eventually leads to a binding curve that approaches the DFT results.

We also make sure that the performance of our linear models are reasonable by comparing their loss metrics to the performance of different neural network potentials trained on the same dataset in [32] in Table I. For the

TABLE I. Comparison of linear ACE models to neural network potentials in MAE for energies and forces for the Carbon dataset in [26] for datasets containing  $n_{\text{set}} = 1000$  and 50000 structures. Energies (E) are in meV/atom and force components (F) are in meV/Å.

Potentials	$n_{\text{set}} = 1000$		$n_{\text{set}} = 50000$	
	E	F	E	F
$K = 4, 250N_f$	48.50	241.27	44.06	222.42
$K = 4, 493N_f$	18.30	199.23	17.55	176.48
$K = 4, 930N_f$	15.40	167.73	15.27	166.70
$K = 5, 793N_f$	14.88	160.78	14.74	159.80
PANNA small	22.40	248.85	17.76	162.37
PANNA mid	20.93	241.36	12.41	137.45
PANNA big	17.88	242.02	8.21	166.95
NequIP $l = 1$	20.40	213.00	7.96	110.00
NequIP $l = 2$	6.83	105.00	5.21	51.40
MACE	6.81	103.14	1.82	51.31

1000-size subsets, we found that the linear ACE models with the most complex descriptor sets ( $K = 4, N_f = 930$  and  $K = 5, N_f = 793$ ) were able to outperform all PANNA potentials and even the  $l = 1$  version of the NequIP [33] potential. However, they perform relatively worse with all other potentials when the complete 50000-size Carbon set is used as the training set, which suggests that the nonlinearities absent in the ACE models provide a considerable improvement in training more complex datasets. Despite this, we assert that the inability of the linear models to capture the effective two-body interaction and converge to a defined shape are not due to the poor  $\mathcal{L}$ , but rather the nature and truncation of the expansion employed in the descriptor sets.

#### IV. SUMMARY AND CONCLUSIONS

In this work, we studied the convergence of linear cluster expansions with respect to the  $N$ -body basis functions through the effective two-body interactions,  $E_{2b}$ , of elemental Carbon systems. We used the atomic cluster expansion (ACE), with descriptor sets truncated at body-orders  $K = 2, 3, 4$  trained on pure dimers, then on two datasets of different diversities but without any dimers. The potentials trained on the dataset limited to diamond structures generally performed poorly: overfitting on training data, and producing a flat dimer curve. The potential trained on a more diverse dataset fared better in the validation errors and resulted in a nontrivial curve dimer curve, but still very far from the theoretical two-body interaction calculated by DFT. Moreover, the dimer curves between descriptor sets clipped at different  $K$  did not seem to converge to a universal function for a given dataset. Even training on the full original dataset led to the same results. We conclude that machine learning potentials employing linear cluster expansions optimize losses at low  $K$ , but fail to generalize and converge properties described by two-body interactions.

A recent study in [34] provides a canonical ACE where self-interactions are removed. Their tests on properties from out-of-domain elements show that while the potentials trained with canonical ACE provides smoother dimers as compared to the ones trained with the self-interacting ACE, the potentials at different regularization tolerances do not stabilize to a single curve. This suggests that the inability of the potentials to converge properties at low  $K$  may go beyond the contributions of the self-interactions and is innate in the expansion itself.

## V. ACKNOWLEDGEMENT

This study was funded by the European Union – NextGenerationEU – PNRR M4C2-I.1.4, in the framework of the project CN-HPC: National Centre for HPC, Big Data and Quantum Computing - Spoke 7 - (MUR ID: CN\_00000013 – CUP: G93C22000600001). FP work was supported by EU – FSE REACT-EU and Italian MUR under contract 45-I-D2100-1 of the PON-RI 2014-2020 initiative. SdG work was supported in part by the European Commission through the MAX Centre of Excellence for supercomputing applications (grant numbers 10109337 and 824143). Computational resources were provided by CINECA.

- 
- [1] R. Drautz, Atomic cluster expansion for accurate and transferable interatomic potentials, *Physical Review B* **99**, 014104 (2019).
- [2] J. Sanchez, F. Ducastelle, and D. Gratias, Generalized cluster description of multicomponent systems, *Physica A: Statistical Mechanics and its Applications* **128**, 334 (1984).
- [3] L. G. Ferreira, S.-H. Wei, and A. Zunger, First-principles calculation of alloy phase diagrams: The renormalized-interaction approach, *Physical Review B* **40**, 3197 (1989).
- [4] F. H. Stillinger and T. A. Weber, Computer simulation of local order in condensed phases of silicon, *Physical Review B* **31**, 5262 (1985).
- [5] R. Biswas and D. R. Hamann, New classical models for silicon structural energies, *Physical Review B* **36**, 6434 (1987).
- [6] J. Tersoff, Modeling solid-state chemistry: Interatomic potentials for multicomponent systems, *Physical Review B* **39**, 5566 (1989).
- [7] J. Behler and M. Parrinello, Generalized Neural-Network Representation of High-Dimensional Potential-Energy Surfaces, *Physical Review Letters* **98**, 146401 (2007).
- [8] A. P. Bartók, R. Kondor, and G. Csányi, On representing chemical environments, *Physical Review B* **87**, 184115 (2013).
- [9] L. Zhang, J. Han, H. Wang, R. Car, and W. E, Deep Potential Molecular Dynamics: A Scalable Model with the Accuracy of Quantum Mechanics, *Physical Review Letters* **120**, 143001 (2018).
- [10] R. Lot, F. Pellegrini, Y. Shaidu, and E. Küçükbenli, PANNA: Properties from Artificial Neural Network Architectures, *Computer Physics Communications* **256**, 107402 (2020).
- [11] A. V. Shapeev, Moment Tensor Potentials: A class of systematically improvable interatomic potentials, *Multiscale Modeling & Simulation* **14**, 1153 (2016), [arXiv:1512.06054](https://arxiv.org/abs/1512.06054) [cond-mat, physics:physics].
- [12] I. Batatia, S. Batzner, D. P. Kovács, A. Musaelian, G. N. C. Simm, R. Drautz, C. Ortner, B. Kozinsky, and G. Csányi, The design space of E(3)-equivariant atom-centred interatomic potentials, *Nature Machine Intelligence* **10.1038/s42256-024-00956-x** (2025).
- [13] I. Batatia, D. P. Kovács, G. N. C. Simm, C. Ortner, and G. Csányi, MACE: Higher Order Equivariant Message Passing Neural Networks for Fast and Accurate Force Fields (2023), [arXiv:2206.07697](https://arxiv.org/abs/2206.07697) [cond-mat, physics:physics, stat].
- [14] F. Musil, A. Grisafi, A. P. Bartók, C. Ortner, G. Csányi, and M. Ceriotti, Physics-Inspired Structural Representations for Molecules and Materials, *Chemical Reviews* **121**, 9759 (2021).
- [15] G. Dusson, M. Bachmayr, G. Csányi, R. Drautz, S. Etter, C. Van Der Oord, and C. Ortner, Atomic cluster expansion: Completeness, efficiency and stability, *Journal of Computational Physics* **454**, 110946 (2022).
- [16] J. Thomas, H. Chen, and C. Ortner, Body-Ordered Approximations of Atomic Properties, *Archive for Rational Mechanics and Analysis* **246**, 1 (2022).
- [17] R. Drautz, M. Fähnle, and J. M. Sanchez, General relations between many-body potentials and cluster expansions in multicomponent systems, *Journal of Physics: Condensed Matter* **16**, 3843 (2004).
- [18] D. P. Kovács, C. V. D. Oord, J. Kucera, A. E. A. Allen, D. J. Cole, C. Ortner, and G. Csányi, Linear Atomic Cluster Expansion Force Fields for Organic Molecules: Beyond RMSE, *Journal of Chemical Theory and Computation* **17**, 7696 (2021).
- [19] Y. Lysogorskiy, C. V. D. Oord, A. Bochkarev, S. Menon, M. Rinaldi, T. Hammerschmidt, M. Mrovec, A. Thompson, G. Csányi, C. Ortner, and R. Drautz, Performant implementation of the atomic cluster expansion (PACE) and application to copper and silicon, *npj Computational Materials* **7**, 97 (2021).
- [20] A. Bochkarev, Y. Lysogorskiy, S. Menon, M. Qamar, M. Mrovec, and R. Drautz, Efficient parametrization of the atomic cluster expansion, *Physical Review Materials* **6**, 013804 (2022).
- [21] M. Qamar, M. Mrovec, Y. Lysogorskiy, A. Bochkarev, and R. Drautz, Atomic Cluster Expansion for Quantum-Accurate Large-Scale Simulations of Carbon, *Journal of Chemical Theory and Computation* **19**, 5151 (2023).
- [22] I. Batatia, P. Benner, Y. Chiang, A. M. Elena, D. P. Kovács, J. Riebesell, X. R. Advincula, M. Asta, M. Avaylon, W. J. Baldwin, F. Berger, N. Bernstein, A. Bhowmik, S. M. Blau, V. Cărare, J. P. Darby, S. De, F. Della Pia, V. L. Deringer, R. Elijošius, Z. El-Machachi, F. Falcioni, E. Fako, A. C. Ferrari, A. Genreith-Schriever, J. George, R. E. A. Goodall, C. P.

- Grey, P. Grigorev, S. Han, W. Handley, H. H. Heenen, K. Hermansson, C. Holm, J. Jaafar, S. Hofmann, K. S. Jakob, H. Jung, V. Kapil, A. D. Kaplan, N. Karimitari, J. R. Kermode, N. Kroupa, J. Kullgren, M. C. Kuner, D. Kuryla, G. Liepuoniute, J. T. Margraf, I.-B. Magdău, A. Michaelides, J. H. Moore, A. A. Naik, S. P. Niblett, S. W. Norwood, N. O'Neill, C. Ortner, K. A. Persson, K. Reuter, A. S. Rosen, L. L. Schaaf, C. Schran, B. X. Shi, E. Sivonxay, T. K. Stenczel, V. Svahn, C. Sutton, T. D. Swinburne, J. Tilly, C. van der Oord, E. Varga-Umbrich, T. Vegge, M. Vondrák, Y. Wang, W. C. Witt, F. Zills, and G. Csányi, A foundation model for atomistic materials chemistry (2024), [arXiv:2401.00096](https://arxiv.org/abs/2401.00096) [cond-mat, physics:physics].
- [23] M. W. Finnis and J. E. Sinclair, A simple empirical N-body potential for transition metals, *Philosophical Magazine A* **50**, 45 (1984).
- [24] J. Tersoff, New empirical approach for the structure and energy of covalent systems, *Physical Review B* **37**, 6991 (1988).
- [25] A. P. Bartók, M. C. Payne, R. Kondor, and G. Csányi, Gaussian Approximation Potentials: The Accuracy of Quantum Mechanics, without the Electrons, *Physical Review Letters* **104**, 136403 (2010).
- [26] Y. Shaidu, E. Küçükbenli, R. Lot, F. Pellegrini, E. Kaxiras, and S. De Gironcoli, A systematic approach to generating accurate neural network potentials: The case of carbon, *npj Computational Materials* **7**, 52 (2021).
- [27] A. R. Oganov and M. Valle, How to quantify energy landscapes of solids, *The Journal of Chemical Physics* **130**, 104504 (2009).
- [28] Y. Eldar, M. Lindenbaum, and M. Porat, The Farthest Point Strategy for Progressive Image Sampling, *IEEE Transactions on Image Processing* (1997).
- [29] P. Giannozzi, S. Baroni, N. Bonini, M. Calandra, R. Car, C. Cavazzoni, D. Ceresoli, G. L. Chiarotti, M. Cococcioni, I. Dabo, A. Dal Corso, S. De Gironcoli, S. Fabris, G. Fratesi, R. Gebauer, U. Gerstmann, C. Gougoussis, A. Kokalj, M. Lazzeri, L. Martin-Samos, N. Marzari, F. Mauri, R. Mazzarello, S. Paolini, A. Pasquarello, L. Paulatto, C. Sbraccia, S. Scandolo, G. Sclauzero, A. P. Seitsonen, A. Smogunov, P. Umari, and R. M. Wentzcovitch, QUANTUM ESPRESSO: A modular and open-source software project for quantum simulations of materials, *Journal of Physics: Condensed Matter* **21**, 395502 (2009).
- [30] R. Sabatini, T. Gorni, and S. De Gironcoli, Nonlocal van der Waals density functional made simple and efficient, *Physical Review B* **87**, 041108 (2013).
- [31] A. Hjorth Larsen, J. Jørgen Mortensen, J. Blomqvist, I. E. Castelli, R. Christensen, M. Dułak, J. Friis, M. N. Groves, B. Hammer, C. Hargus, E. D. Hermes, P. C. Jennings, P. Bjerre Jensen, J. Kermode, J. R. Kitchin, E. Leonhard Kolsbjerg, J. Kubal, K. Kaasbjerg, S. Lysgaard, J. Bergmann Maronsson, T. Maxson, T. Olsen, L. Pastewka, A. Peterson, C. Rostgaard, J. Schiøtz, O. Schütt, M. Strange, K. S. Thygesen, T. Vegge, L. Vilhelmsen, M. Walter, Z. Zeng, and K. W. Jacobsen, The atomic simulation environment—a Python library for working with atoms, *Journal of Physics: Condensed Matter* **29**, 273002 (2017).
- [32] F. Pellegrini, R. Lot, Y. Shaidu, and E. Küçükbenli, PANNA 2.0: Efficient neural network interatomic potentials and new architectures, *The Journal of Chemical Physics* **159**, 084117 (2023).
- [33] S. Batzner, A. Musaelian, L. Sun, M. Geiger, J. P. Mailoa, M. Kornbluth, N. Molinari, T. E. Smidt, and B. Kozinsky, E(3)-equivariant graph neural networks for data-efficient and accurate interatomic potentials, *Nature Communications* **13**, 2453 (2022).
- [34] C. H. Ho, T. S. Gutleb, and C. Ortner, Atomic Cluster Expansion without Self-Interaction (2024), [arXiv:2401.01550](https://arxiv.org/abs/2401.01550) [physics].

# Supporting information for: Convergence of body-orders in linear atomic cluster expansions

Apolinario Miguel Tan,<sup>\*</sup> Franco Pellegrini, and Stefano de Gironcoli

*Scuola Internazionale Superiore di Studi Avanzati, Trieste, Italy*

E-mail: atan@sissa.it

## A. Simulation Parameters

For all runs: The cutoff is set to 5 Å for both the force and neighbor list cutoffs. The potential does not use the nonlinear version of the Finnis-Sinclair potential which is set on by default in the pacemaker package. The radial basis is the Chebyshev expansion with cosine cutoff function. The energy-force cost balancing is set that the RMSE for forces is weighted 50 times more than the energies. The optimizer is set to BFGS with a maximum of 3000 iterations and a batch size of 100. Details about the input files may be found at the documentation of pacemaker.

Table 1 distinguishes the training parameters done for the dimer curves presented in the main paper.

Table 1: Simulation Parameters for binding curve experiments

Training set	Descriptor label	Train steps	Validation set	nmax	lmax
Dimer 124	$K = 2, N_f = 45$	3000	val_dimer 123	100	0
	$K = 3, N_f = 90$	3000	val_dimer 123	45/8	0/2
	$K = 4, N_f = 250$	3000	val_dimer 123	45/5/4	0/2/2
Diamond 1000	$K = 2, N_f = 45$	3000	val_diverse 123	100	0
	$K = 3, N_f = 90$	3000	val_diverse 123	45/8	0/2
	$K = 4, N_f = 250$	3000	val_diverse 123	45/5/4	0/2/2
Diverse 1000	$K = 2, N_f = 45$	3000	val_diverse 1000	100	0
	$K = 3, N_f = 90$	3000	val_diverse 1000	45/8	0/2
	$K = 4, N_f = 250$	3000	val_diverse 1000	45/5/4	0/2/2
	$K = 4, N_f = 493$	3000	val_diverse 1000	45/8/4	0/3/3
	$K = 4, N_f = 960$	3000	val_diverse 1000	45/9/5	0/6/3
	$K = 4, N_f = 793$	3000	val_diverse 1000	45/8/4/3	0/3/3/2
Diverse 50000	$K = 4, N_f = 250$	3000	val_diverse 1000	45/5/4	0/2/2
	$K = 4, N_f = 493$	810	val_diverse 1000	45/8/4	0/3/3
	$K = 4, N_f = 960$	418	val_diverse 1000	45/9/5	0/6/3
	$K = 4, N_f = 793$	1151	val_diverse 1000	45/8/4/3	0/3/3/2

## B. Additional plots

### B.1. Force plots between DFT and dimer-trained potential

Fig. 1 shows the force values from the reference DFT data (blue scatter) as compared with the values predicted by the NNP (orange line) at the short-range region for the dimer-trained potential with  $K = 4$  and  $N_f = 250$ . We see that despite relatively low relative errors (maximum at 13%), the absolute value of the forces admit large errors which contribute to the large validation errors at the overfitting region.



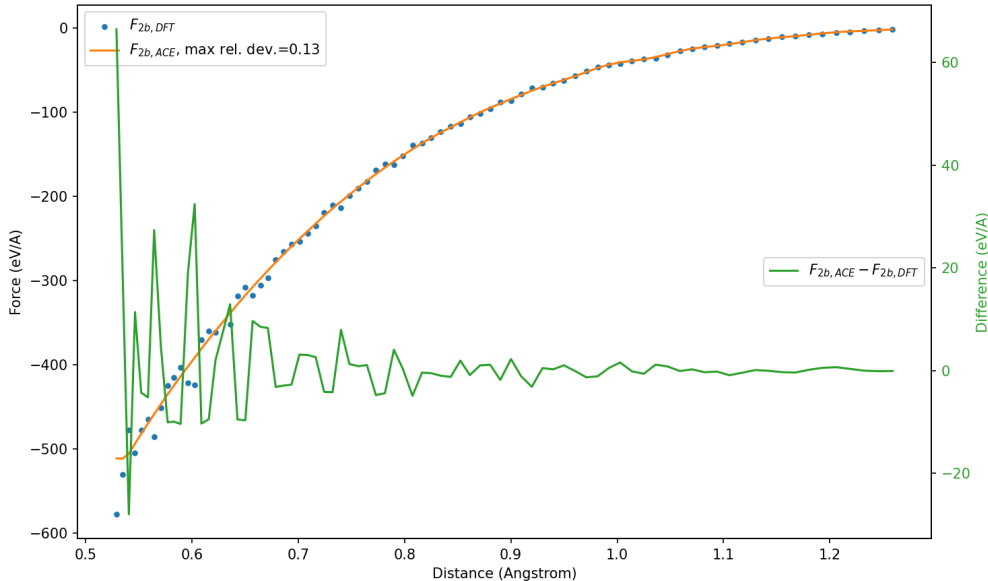


Figure 1: Forces at the short-range region for the dimer-trained potential and the difference between the forces of the DFT and the dimer-trained potential (green, right y-axis).

## B.2. Loss analysis of diverse dataset dimer curves

Fig. 2 (top) shows the loss  $\mathcal{L}$  vs. number of functions  $N_f$  for the potential trained on the diverse dataset and (bottom) the corresponding dimer curves at the terminal  $N_f$  for each body-order  $K$ . We see from the loss curves that opening the channel for more complex basis functions by increasing  $K$  does help improve training. Further evidence of this comes from the faint lines, which are loss data from potentials still trained with  $K = 2$  (or  $K = 3$ ) but have the same number of functions as the next higher  $K$ . Despite that, the dimer curve shows that there is a more prominent qualitative change going from  $K = 2$  to  $K = 3$  rather than from  $K = 3$  to  $K = 4$  despite having a smaller drop in losses. From here we see that the parameters at which the loss converges do not indicate that the curves have already converged.

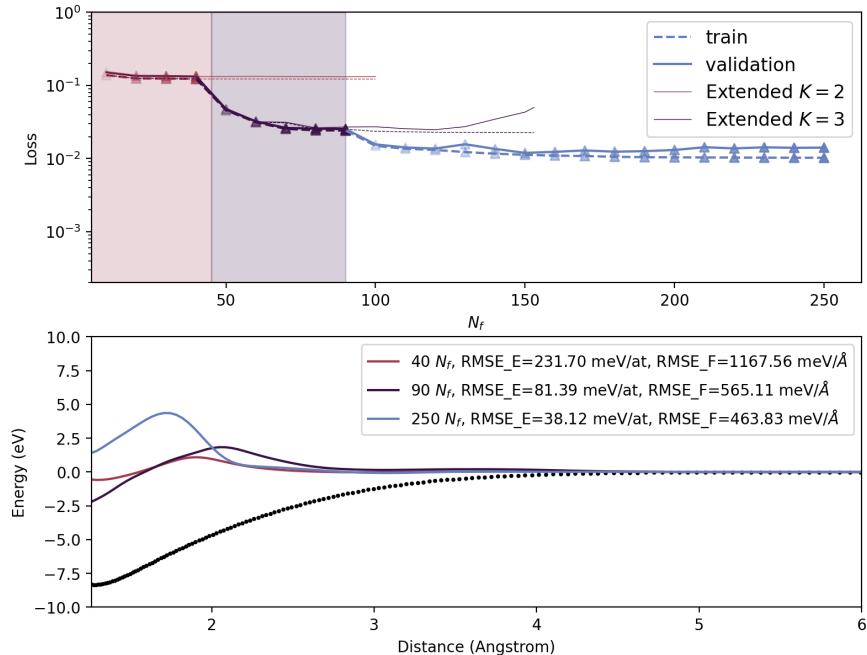


Figure 2:  $\mathcal{L}$  vs.  $N_f$  (top) and dimer curves (bottom) for the diverse dataset. Orange and pink plots correspond to potentials with only  $K = 2$  and up to  $K = 3$  functions, respectively while purple curves include  $K = 4$  functions. The x-values of the dimer curve start at the minimum distance found in the homogeneous dataset.

### B.3. Biasing the diverse dataset with dimer data

Fig. 3 shows the effect of biasing the diverse dataset with an increasing number of dimer structures. These tests were done to verify that the linear ACE potentials is very much capable of learning the correct interaction curve if sufficient data is provided. We show that once around 10% of the dataset is composed of dimer structures, the potential is able to approach the DFT data. We also added an additional potential trained on the dataset with 50 dimers added but initialized with a different seed to ensure that initialization effects are minimal.

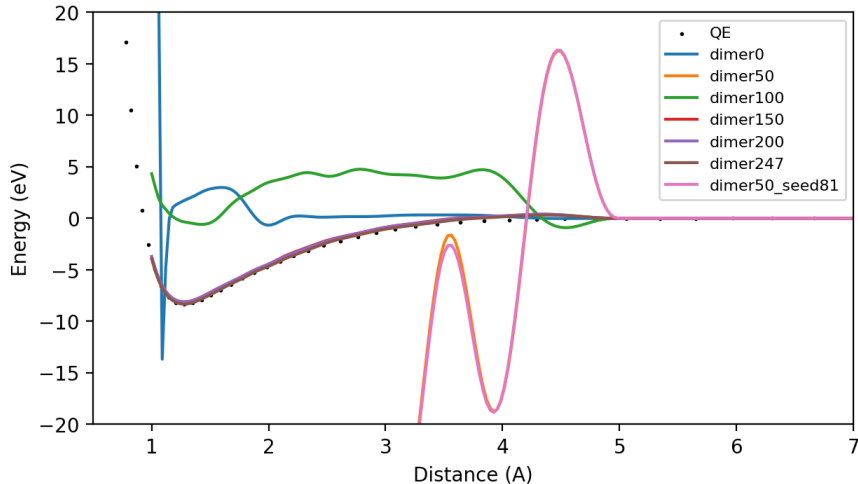


Figure 3: Dimer curves of potentials trained from the mixture of the 1000 structures from the diverse dataset with an increasing number of structures from the dimer dataset. An additional potential was also trained on the dataset with 50 dimers added but initialized with a different seed to check the initialization effects. Prominent oscillations at short-range are due to absence of bond pairs in structures in the dataset at the sub-1 Å distance region.

#### B.4. Learning curves of diverse dataset runs

Figs. 4 and 5 show the learning rates for the diverse dataset with 1000 and 50000 structures, respectively. The different colors indicate the descriptor sets of varying complexity and body-order as controlled by  $K$  and  $N_f$ . In general, we see that the potentials trained by the dataset with fewer structures approach the overfitting regions much faster and indicate that less complex descriptor sets, which have less parameters, are less susceptible to overfitting. On the other hand, the potentials trained with 50 times the data as compared previously still haven't overfit. Both learning curves have losses around the same order of magnitude, which indicates that the larger dataset benefits from the more complex descriptor sets<sup>1</sup>.

<sup>1</sup>We did not train for longer as it would be computationally expensive without the promise that the losses and dimer curves would have improved by then.

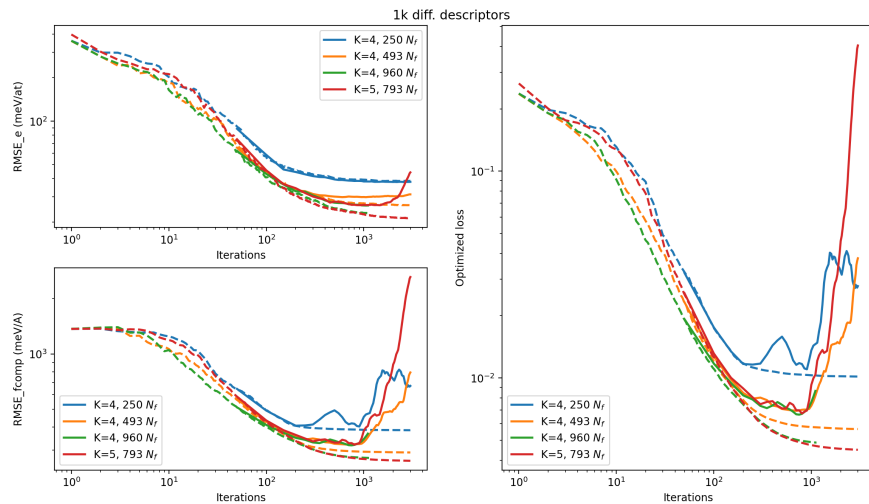


Figure 4: Learning rates for (upper left) energy, (lower left) force, and (right) total for the diverse dataset with 1000 structures. Different colors indicate different descriptor sets with varying  $K$  and  $N_f$ .

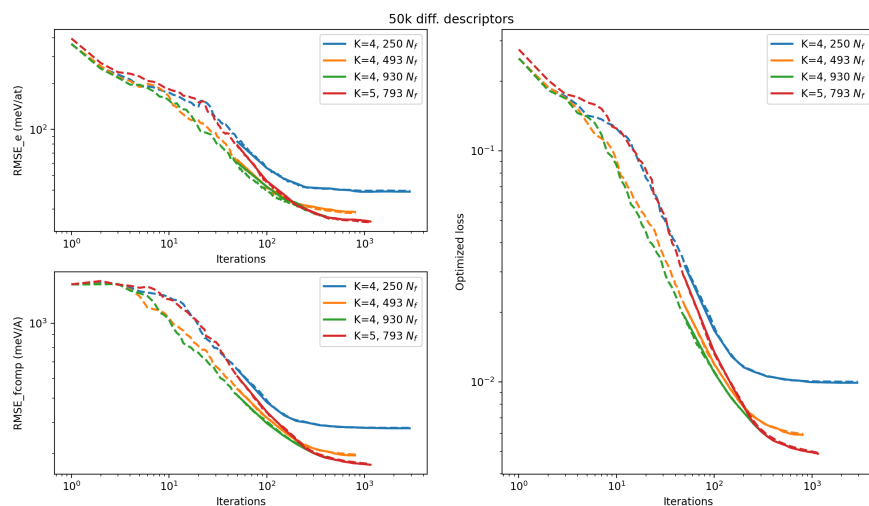


Figure 5: Learning rates for (upper left) energy, (lower left) force, and (right) total for the diverse dataset with 50000 structures.

## B.5. Learning curves and dimer curves for 5k and 10k runs

Figs. 6 and 7 show the learning rates for the diverse dataset with 5000 and 10000 structures, respectively. The different colors indicate the descriptor sets of varying complexity and body-order as controlled by  $K$  and  $N_f$ . Less prominent overfitting is observed in the 5000 dataset as compared to the learning curve of the potentials trained on the 1000-structure dataset. The learning curves of the 10000 dataset do not show any signs of overfitting after the runs were completed. Their corresponding dimer curves in Fig. 8 and 9 show similar behavior from the potentials trained from the 1000 and 50000 structures in that the dimer curves do not approach a defined curve as higher  $K$  basis functions are introduced in the descriptor set.

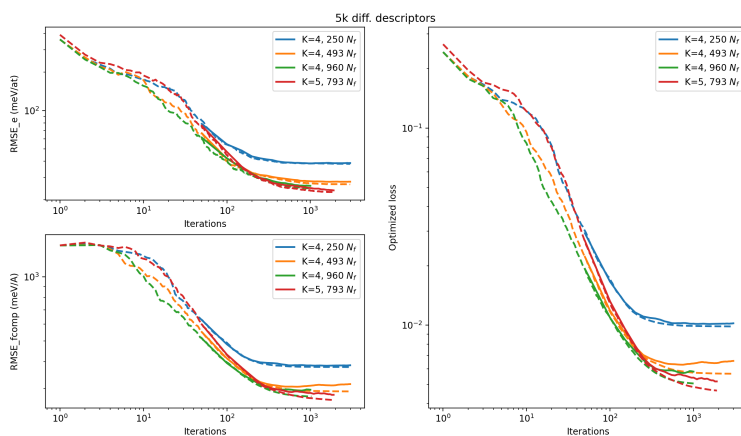


Figure 6: Learning rates for (upper left) energy, (lower left) force, and (right) total for the diverse dataset with 5000 structures. Different colors indicate different descriptor sets with varying  $K$  and  $N_f$ .

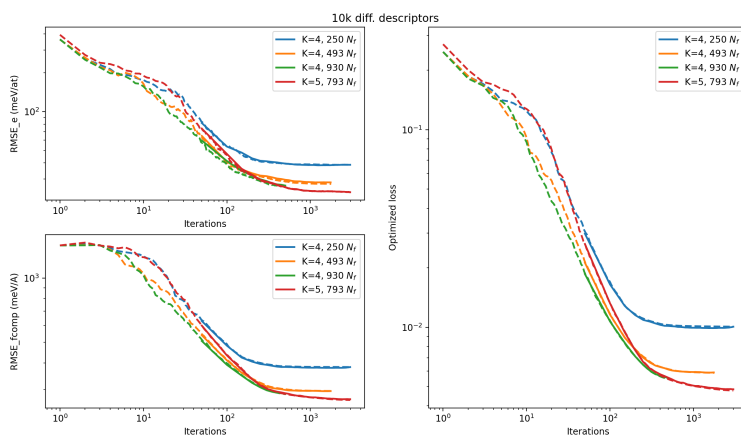


Figure 7: Learning rates for (upper left) energy, (lower left) force, and (right) total for the diverse dataset with 10000 structures.

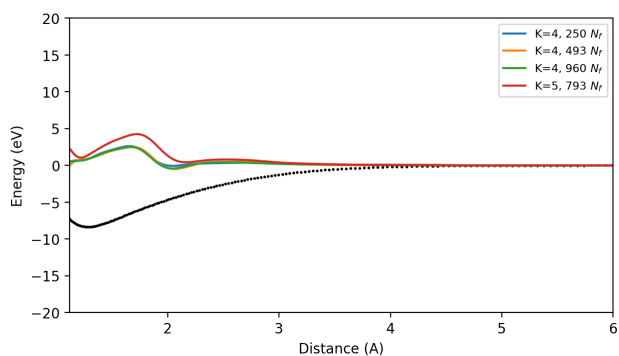


Figure 8: Dimer curves for the diverse dataset with 5000 structures. Different colors indicate different descriptor sets with varying  $K$  and  $N_f$ .

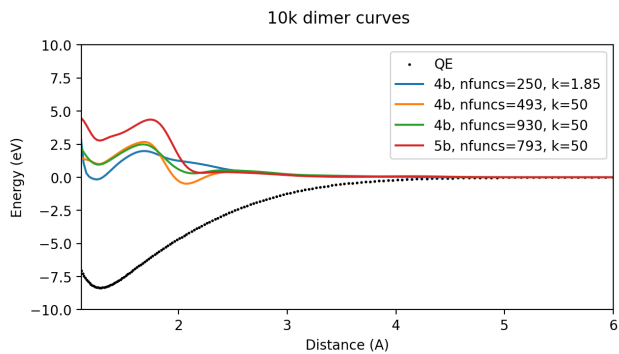


Figure 9: Dimer curves for the diverse dataset with 10000 structures. Different colors indicate different descriptor sets with varying  $K$  and  $N_f$ .